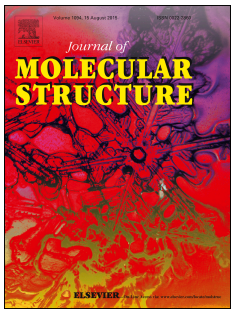


# Synthesis, crystal structure, hirshfeld surface analysis, DFT calculations, anti-diabetic activity and molecular docking studies of (*E*)-*N*′-(5-bromo-2-hydroxybenzylidene) isonicotinohydrazide

Khalid Karrouchi, Saad Fettach, Mukesh M. Jotani, Abir Sagaama, Smaail Radi, Hazem A. Ghabbour, Yahia N. Mabkhot, Benacer Himmi, My El Abbes Faouzi, Noureddine Issaoui

PII: S0022-2860(20)31125-X

DOI: https://doi.org/10.1016/j.molstruc.2020.128800

Reference: MOLSTR 128800

To appear in: *Journal of Molecular Structure*

Received Date: 27 April 2020

Revised Date: 25 June 2020

Accepted Date: 29 June 2020

Please cite this article as: K. Karrouchi, S. Fettach, M.M. Jotani, A. Sagaama, S. Radi, H.A. Ghabbour, Y.N. Mabkhot, B. Himmi, M. El Abbes Faouzi, N. Issaoui, Synthesis, crystal structure, hirshfeld surface analysis, DFT calculations, anti-diabetic activity and molecular docking studies of (*E*)-*N*′-(5-bromo-2-hydroxybenzylidene) isonicotinohydrazide, *Journal of Molecular Structure* (2020), doi: https://doi.org/10.1016/j.molstruc.2020.128800.

# CRediT author Statement

**Khalid Karrouchi:** Conceptualization, Methodology, Original Draft, Writing - Review & Editing.

**Saad Fettach:** Methodology, Investigation.

**Mukesh M. Jotani:** Theoretical, Calculations Writing - Original Draft.

**Abir Sagaama:** Methodology, Investigation.

**Smaail Radi:** Supervision, Project administration.

**Hazem A. Ghabbour:** Software, Formal analysis.

**Yahia N. Mabkhot:** Software, Formal analysis.

**Benacer Himmi:** Investigation.

**My El Abbes Faouzi :** Visualization, Investigation.

**Noureddine Issaoui:** Theoretical, Calculations Writing - Original Draft, Writing - Review & Editing.

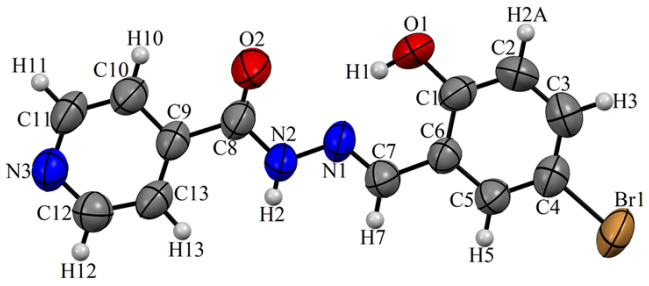


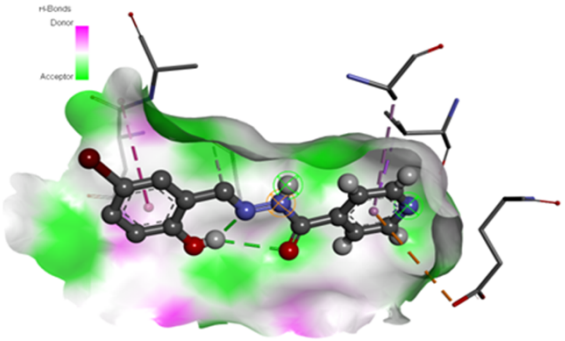


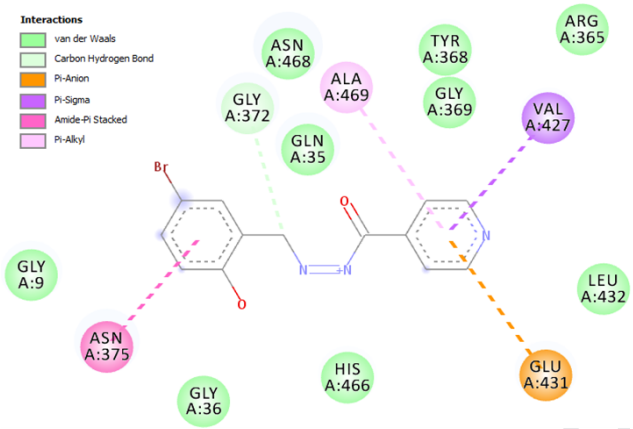


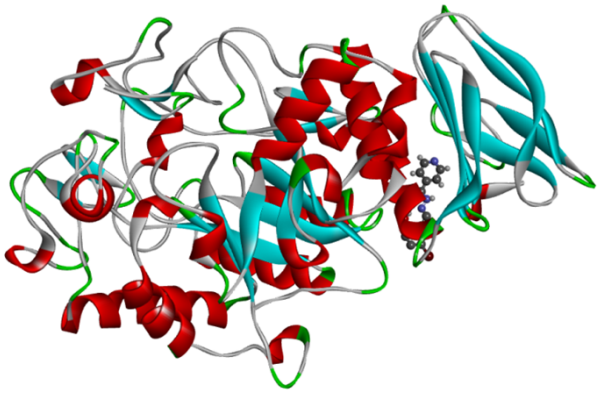

# Synthesis, crystal structure, hirshfeld surface analysis, DFT calculations, anti-diabetic activity and molecular docking studies of (*E*)-*N'*-(5-bromo-2-hydroxybenzylidene) isonicotinohydrazide

Khalid Karrouchi [a,*], Saad Fettach [b], Mukesh M. Jotani [c], Abir Sagaama [d], Smaail Radi [e], Hazem A. Ghabbour [f], Yahia N. Mabkhot [g,h], Benacer Himmi [i], My El Abbes Faouzi [b], Noureddine Issaoui [d,*]

[a]*Laboratory of Analytical Chemistry and Bromatology, Faculty of Medicine and Pharmacy, Mohammed V University, Rabat, Morocco.*

[b]*Biopharmaceutical and toxicological analysis research team, Laboratory of Pharmacology and Toxicology, Pharmacokinetic Research Team, Faculty of Medicine and Pharmacy, University Mohammed V of Rabat, Morocco.*

[c]*Department of Physics, Bhavan's Sheth R. A. College of Science, Ahmedabad, Gujarat 380001, India*

[d]*University of Monastir, Laboratory of Quantum and Statistical Physics (LR18ES18), Faculty of Sciences, Monastir 5079, Tunisia.*

[e]*Laboratoire de Chimie Appliquée et Environnement (LCAE), Faculté des Sciences, Université Mohamed I, 60000 Oujda, Morocco.*

[f]*Department of Pharmaceutical Chemistry, College of Pharmacy, King Saud University, P. O. Box 2457, Riyadh 11451, Saudi Arabia.*

[g]*Departement of Pharmaceutical Chemistry, College of Pharmacy, King Khalid University, Abha 61421, P. O. Box 960, 61421, Saudi Arabia.*

[h]*Research Center for Advanced Materials Science (RCAMS), King Khalid University, Abha 61413, P. O. Box 9004, Saudi Arabia.*

[i]*Filière Techniques de Santé, Institut Supérieur des Professions Infirmières et Techniques de Santé de Rabat, Ministère de la Santé, Morocco.*

*Corresponding authors:

Khalid.karrouchi@um5s.net.ma (K. Karrouchi)

issaoui_noureddine@yahoo.fr (N. Issaoui)

**Abstract**

In this present work, the newly synthesized compound *E*)-N'-(5-bromo-2-hydroxybenzylidene)isonicotinohydrazide (**2**) has been synthesized and characterized by IR, $^{1}H$ &$^{13}C$ NMR, ESI-MS and single crystal X-ray diffraction analysis using experimental and theoretical methods. The molecular geometry, vibrational frequencies, frontier molecular orbital (HOMO-LUMO) energies and thermodynamic properties of the title molecule were explored using Density Functional Theory (DFT) calculation via B3LYP method with 6-31++G (d,p) basis set. Moreover, Hirshfeld and Molecular electrostatic potential (MEP) surfaces analyses were investigated. In addition, the title compound was evaluated for their *in vitro* antidiabetic activity against α-glucosidase and α-amylase enzymes. Finally, Molecular docking studies were performed between the title ligand and 1CLV/2ZE0 enzymes. Docking calculations showed that the **2**-2ZE0 complex is more stable than **2**-1CLV complex, since it has the best inhibitory impact whose their total energy score equal to -108.68 Kcal/mol. Docking results reveal that the main interaction forces are H-bond and van der Waals interactions.

**Keywords:** Isoniazid; X-ray analysis; DFT; Hirshfeld surface analysis; α-glucosidase; α-amylase; Molecular docking.

## 1. Introduction

Diabetes mellitus is a serious metabolic disorder of modern era and severe interminable health complications are associated with it, and type-2 diabetes is widely spread kind of this disorder [1]. Hence, one of the therapeutic approaches in treating diabetes is to reduce postprandial hyperglycemia by inhibiting major carbohydrate hydrolyzing enzymes. Two enzymes have been implicated in processes leading to the development of diabetic symptoms, namely α-glucosidase, which is also implicated in intestinal disease and α-amylase, which hydrolyzes α-bonds of large α-linked polysaccharides. These enzymes are the key carbohydrate hydrolyzing enzymes, located in the brush-border surface membrane of human intestinal cells, which plays an important role in the carbohydrate digestion [2, 3]. Thus, discovery and development of new α-glucosidase and α-amylase inhibitors have attracted great attention in recent years [4, 5].

The N-acylhydrazone scaffold (-CO-NH-N=CH-) is represented by the fusion between imine and amide subunits, which provides pharmacophoric interaction points including both hydrogen-bond donor and acceptors sites and are capable of interacting with a large range of active sites [6, 7]. Generally, the *N*-acylhydrazones are prepared by condensation of ketones,

or aldehydes with hydrazides [8-10]. Changes of the subunits bonded to both acyl and imine functions resulted in several *N*-acylhydrazone derivatives that are capable to modulate different molecular targets, providing a surprisingly wide range of pharmacological activities such as antiviral, analgesic, antimicrobial, anti-inflammatory, anti-cancer, antioxidant, vasodilator, trypanocidal, antiplatelet, antiprotozoal, cathecolase and antinociceptive agents [11-23].

Given the importance of therapeutic properties of *N*-acylhydrazone derivatives, the study of the molecular structure, electronic and thermodynamic properties are essential to know the effect of different substituents on molecular structures in order to find the relationship of these groups with their biological activities. In this context, DFT calculations have become a very important and widely used tool to develop a close relationship between theoretical and experimental data by giving clues related to molecular geometry structure and to electronic and thermodynamic properties. Consequently, these techniques have become very reliable in the prediction of many molecular properties with great precision [24-30].

In this study, we report the synthesis (*E*)-*N'*-(5-bromo-2-hydroxybenzylidene) isonicotino-hydrazide to be evaluated as a new anti-diabetic agent. The newly synthesized compound was characterized by IR, $^{1}$H- and $^{13}$C-NMR, ESI-MS and the (*E*)-configuration of azomethine (N=CH) group was confirmed by single-crystal X-ray diffraction analysis. In addition, the molecular geometry, HOMO-LUMO energies, molecular electrostatic potential (MEP) and thermodynamic properties of the title molecule were explored using DFT/B3LYP method with 6-31++G (d,p) basis set. The *in vitro* antidiabetic activity of the target compound was evaluated against two enzymes α-glucosidase and α-amylase. Finally, Molecular docking studies were performed between the title ligand and 1CLV/2ZE0 enzymes.

## 2. Experimental

### *2.1. General methods*

Chemical reagents were purchased from Fluka, Sigma and Aldrich chemicals. Reactions were checked with TLC using aluminum sheets with silica gel 60 F254 from Merck. Melting points were measured using a Buchi B-545 digital capillary melting point apparatus and used without correction. The FT-IR spectrum was recorded with Perkin-Elmer VERTEX 70 FT-IR spectrometer covering field 400–4.000 $cm^{-1}$. NMR spectroscopies were recorded in dry

deuterated DMSO on a Bruker AC spectrometer at 200 MHz for $^{1}$H NMR and 50 MHz for $^{13}$C NMR; δ is expressed in ppm related to TMS (0 ppm) as internal standard. Splitting patterns are designated as follow: s (singlet), d (doublet), t (triplet), m (multiplet). Coupling constants (*J* values) are listed in Hertz (Hz). Mass spectra were obtained using an API 3200 LC/MS/MS system equipped with an ESI source and the samples were diluted in methanol.

### *2.2. Synthesis*

*General procedure for the synthesis of (E)-N'-(5-bromo-2-hydroxybenzylidene)isonicotino-hydrazide* (**2**)

The title compound was prepared according to the previously published protocol [31-33]. (Scheme 1).To a solution of Isoniazid (137 mg, 1 mmol) and 5-bromo-2-hydroxybenzaldehyde (201 mg, 1 mmol) in 10 ml of ethanol was added two drops acetic acid. Then, the reaction mixture was poured in cold water, and the precipitate formed was filtered out and recrystallized from ethanol to afford the product (**2**) as yellow crystals. Yield (75%); m.p. 252-254 °C; IR (ν(cm$^{-1}$)) : 3173 (NH), 3138 (OH), 1675 (C=O), 1613 (C=N); $^{1}$H NMR (200 MHz, DMSO-$d_6$) δ : 12.37 (s, 1H, -CONH-), 11.15 (s, 1H, OH), 8.81 (d, J = 6.1 Hz, 1H, H2 & H6 pyridyl), 8.66 (s, 1H, N=CH), 7.86 (d, J = 6.1 Hz, 1H, H3 & H5 pyridyl), 7.83 (d, J = 2.5 Hz, 1H, H6-Ar), 7.44 (dd, J = 8.8, 2.6 Hz, 1H, H4-Ar), 6.92 (d, J = 8.7 Hz, 1H, H3-Ar).$^{13}$C NMR (50 MHz, DMSO-$d_6$) δ : 160.96, 155.94, 149.84, 145.87, 139.36, 133.36, 129.64, 121.00, 120.75, 118.17, 110.03; ESI-MS: m/z = 320.3[M+H]$^{+}$, m/z = 342.3 [M+Na]$^{+}$.

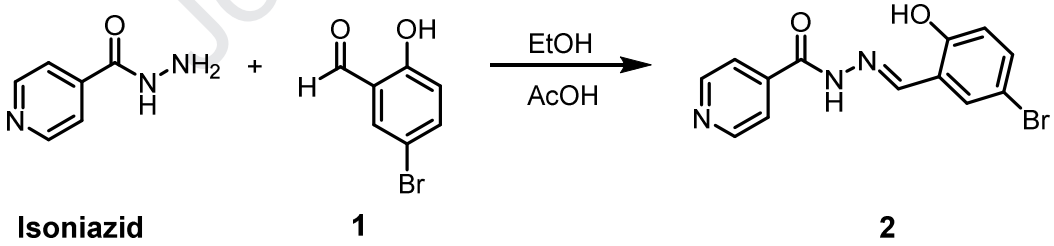


**Scheme 1**. Synthesis of the title compound **2**.

### *2.3. X-ray analysis*

X-ray single crystal data were collected by using graphite monochromatic MoKα radiation (λ = 0.71075 Å) radiation on a Bruker APEX-II D8 Venture area diffractometer. Bruker SAINT was harnessed for data reduction and cell refinement and SHELXT [34, 35] was utilized for structure solving. Full-matrix least-square technique was utilized for final refinement with the

aid of anisotropic thermal data for non-hydrogen atoms on F. The details of the X-ray crystal data and the structure solution as well as the refinement are given in Table 1.

### 2.4. Computational details

#### 2.4.1. DFT

All geometry optimizations and frequency calculations of the desired product **2** were carried out using the Gaussian 09 software [36] and visualizations of modeling were performed with GaussView5 software [37]. The GaussView5 program is designed for the 3-D design of the molecule and to visually identify the properties of the molecule. Density functional theory with the Becke three parameters hybrid functional (DFT-B3LYP/6-31++G (d,p)) [38, 39]. calculations were performed for all atoms of the title compound in the gas phase and DMSO, separately. Vibrational frequencies were calculated at the same level to ensure that each stationary point was a true minimum. The optimized molecular structure is used to perform harmonic vibrational frequencies, NMR shifts and UV-Vis data, HOMO and LUMO distributions and MEP analysis of the studied compound.

#### 2.4.2. Molecular docking studies

Analysis for the docking simulation two programs was used: iGEMDOCK [40] and Discovery Studio Visualizer [41]. The first software gives the total energy value on the basic of the proteins-ligand interactions. Molecular docking parameters selected for iGEMDOCK program were as follows: population size 800, generations 80 and number of solutions 10. The second software determines the representation of the best docked poses of ligand inside protein and their different interactions (VDW, H-bond…). The protein structure of α-glucosidase GSJ enzyme (pdb: 2ZE0) [42] and $\alpha$-amylase (pdb: 1CLV) [43] were download from the Research Collaboratory for Structural Bioinformatics (RSCB) Protein Data Bank (http://www.pdb.org/pdb/home/home.do).

### 2.5. Antidiabetic activity

The α-glucosidase and α-amylase inhibition assays were carried out according to the previously published methods [23, 44].

## 3. Result and discussion

### 3.1. X-ray structure description and optimized geometry

The details of the X-ray crystal data and the structure solution as well as the refinement of the title compound are given in Table 1. Supplementary data are deposited at CCDC under

deposition number 1836618. The title compound crystalized in the monoclinic system, space group $P2_1/c$. The molecular structure of **2** sees (5-bromo-2-hydroxy benzylidene) linked with isonicotine through hydrazine, Fig. 1. The benzylidene-C9 and carbonyl-C8 atoms have the trans configuration about N1-N2 bond characterized from the value of torsional angle C7-N1-N2-C8 to be 176.3(2)°. The twist of (C1-C6) ring about C3-C7 (N1-C7-C3-C4 = -5.2(3) ° and that of N3-containing pyridine ring about C8-C9 bond as the torsion angle of 24.0(3)° had resulted 11.16(11)° dihedral angle between these two aromatic residues. The hydroxyl oxygen atom O1 and bromine Br1 areout of least square plane of (C1-C6) benzene ring and have the deviation of 0.035 Å and -0.034 Å respectively.

The molecular packing of the title molecule features intermolecular hydrazinyl-N—H···N (pyridyl) hydrogen bond which give rise to C(8) chain, whereas the intramolecular hydroxyl-O—H···N (hydrazine) forms S(6) graph-set motif (Fig S1, Table 2). Further, the stability to the layers is provided by aromatic cycle stacking between inversion related (C1-C6) benzene and N3-containing pyridin rings [inter-centroid distance = 3.6712(13) Å at (-x, -y,-z)]. The intermolecular benzene-C—H···π(benzene) contacts between the layers, Table 1, had resulted the three-dimensional architecture in the crystal of **2**.

The optimized geometry of compound **2** is illustrated in Fig. 2. A summary of selected bond lengths [Å] and angles [°] compared to the experimental data on the crystal structure are given in Table 3. The molecular structure of the title compound composed of two rings. These rings are pyridine and 5-bromo-2-hydroxybenzyl which are connected through an acylhydrazone (-CO-NH-N = CH-) group. In the following discussion, the molecular structure and atomic numbering scheme adopted for the present study was taken from the optimized structure (Fig. 2 and Table 3). The C-C bond lengths in the pyridine ring are reported [45] at the range 1.390-1.402 Å and in the present study, The C-C bond lengths (XRD/DFT) are found at the range 1.377-1.503 Å/1.392-1504Å. The C-N bond length is found at 1.344 Å for C22-N6 and 1.333 Å for C24-N6 by XRD, these values are very closer to the calculated values 1.338 Å and 1.335 Å, respectively. In this molecule, the calculated C─C bond length of the benzyl ring varies from 1.382-1.418 Å, which is slightly greater than that of experimental values (1.373-1.403 Å). In carbohydrazide group, the bond length of C18-O3, C18-N5, N4-N5, C16-N4 and C18-C19 are calculated 1.212, 1.358, 1.385, 1.286 and 1.504 Å. The experimental bond lengths of above are observed about 1.205, 1.370, 1.375, 1.275 and 1.503 Å.The calculated N─H bond length in carbohydrazide group is N5─H28 = 1.015 Å by DFT method, which is 0.206 Å deviate from the experimental value (0.809 Å).The calculated C─H bond

length of the 5-bromo-2-hydroxybenzyl and pyridine ring varies from 1.083-1.086 Å which is slightlygreater than that of experimental values (0.930 Å).In the pyridine moiety of the title compound, the bond angles (XRD/DFT) C19-C20-C22, C20-C19-C26and C26-C24-N6 are 118.7°/118.7°, 118.1°/118.0° and 124.1°/123.6°, respectively. For benzyl ring, the bond angles lie between 118.9-120.7° experimentally, these bond angles were predicted at the range 119.1-121.0° with DFT-B3LYP/6-31++G (d,p). From the results we can say that, the DFT/B3LYP functional/method estimated the bond lengths and bond angles in good agreement with experimental results.

### 3.2. FT-IR study

The experimental infrared spectrum of the title compound was recorded in a solid state using reflectance (ATR) mode (Fig. 3). The OH and NH stretching vibrations are generally observed around 3500–3300 $cm^{-1}$ [46]. This absorption is strongly influenced by the chemical environment, in particular when OH or NH groups are involved in the intramolecular or intermolecular hydrogen bond [46]. González-Baró *et al.* [47] reported the NH stretching mode ($\nu_{NH}$) of the isonicotinoylhydrazone of 2-hydroxy-3-methoxybenzaldehyde at 3157 $cm^{-1}$.On the other hand, the intermolecular bond H leads in many cases to a broadening of the band, as shown by the IR spectrum in the case of NH absorption of the title molecule, which has been attributed to the low IR band at 3173 $cm^{-1}$.

Benković *et al.* [48] reported the stretching of the OH groups, involved in the intramolecular hydrogen bond with the nitrogen atom of the group C=N, of hydrazones with hydroxyl groupin position 2 of phenyl ring at 3142 $cm^{-1}$. In the present study, the IR band appears at 3138 $cm^{-1}$ has been assigned to stretching modes of OH involved in the intramolecular hydrogen bond. In general, the OH in-plane deformation vibration for phenols lies in the region 1440-1260 $cm^{-1}$ [49], Arunagiri *et al.* [50] reported the in-plane deformation vibrations of two OH at 1242 and 1220 $cm^{-1}$. In this work, the observed in-plane deformation vibrations of OH appear at 1285 $cm^{-1}$. The in-plane and out-of-plane deformation vibrations of NH modes are observed at 1210 and 875 $cm^{-1}$, respectively [51]. In our present study, the bands observed at 1210 and 888 $cm^{-1}$ is assigned as these modes.

The C-H stretching vibrations of aromatic rings give rise to bands in the region 3200–3000 $cm^{-1}$ in aromatic compounds [52]. For the title molecule, a series of infrared absorptions between 3115 and 2819 $cm^{-1}$ were assigned as CH stretching modes of the pyridyl and benzyl rings. The C-H in-plane deformation vibrations are observed in the region 1300–1000 $cm^{-1}$ and are usually of medium to weak intensity [52]. Galić *et al.* [53] reported the in-plane CH

deformations of the pyridyl and phenyl moieties in the range of 1200–1000 $cm^{-1}$, and the out of plane CH deformations and the skeletal torsions of the aromatic rings between 1000 and 700 $cm^{-1}$. In the present work, the bands due to C-H in-plane bending vibration interact somewhat with C–C stretching vibrations, are observed as a number of bands in the region 1330 and 1067 $cm^{-1}$ in IR. The out-of-plane CH deformations are observed between 600 and 900 $cm^{-1}$ [52]. Generally, the CH out-of-plane deformations with the highest wavenumbers are weaker than those absorbing at lower wavenumber. In our case, the observed wavenumbers with weak intensity at 956, 931, 869 and 704 $cm^{-1}$ are identified as CH out-of-plane deformation vibration.

The C=O stretching vibrations generally appear in a wave number region between 1800–1600 $cm^{-1}$, they are one of the most representative in an infrared spectrum [52]. In our study, the strongest band in the infrared spectrum, at 1675 $cm^{-1}$, is attributed to C=O stretching vibrations. This mode was assigned at 1655 $cm^{-1}$ by Sheeja *et al.* [51] for quinoline-2-carbaldehyde benzoyl hydrazine and at 1656 $cm^{-1}$ by de Freitas *et al.* [46] for 8-hydroxyquinoline-2-carboxaldehyde isonicotinoylhydrazone. The in-plane and out-of-plane deformation vibrations of C=O are expected in the regions 625 ± 70 and 540 ± 80 $cm^{-1}$, respectively [51]. Here, these modes are observed at 779 and 611 $cm^{-1}$ respectively.

The stretching vibrations $\nu_{C=N}$ reported at 1604 and 1603 $cm^{-1}$by Galić *et al.* [53] for aroylhydrazones and the moderate bands at 1364 and 1367 $cm^{-1}$ are assigned as the C-N stretching. For the title molecule, the C=N stretching mode is observed at 1619 $cm^{-1}$ and the medium band observed at 1379 $cm^{-1}$ in the IR spectrum is assigned as C-N stretching mode. The N─N stretching has been reported at 1156 $cm^{-1}$ by de Freitas *et al.* [46], at 1118 $cm^{-1}$ by Sheeja*et al.* [51] and at 1112 $cm^{-1}$ by Arunagiri *et al.* [50]. For our title compound $\nu_{N-N}$ vibrations observed at medium intensity band 1052 $cm^{-1}$ in IR spectrum.The aromatic C=C-C stretching vibrations of phenyl and pyridyl are very much important and occur in the region 1200-1650 $cm^{-1}$ [46]. In this case, the infrared bands at 1411, 1434, 1476, and 1554 $cm^{-1}$ are assigned as C=C stretching mode in pyridyl and phenyl rings (Fig. S1).

### 3.3. $^{1}$H- and $^{13}$C-NMR studies

The $^{1}$H NMR spectra of the title molecule displayed a two doublets at δ 6.92 and 7.83 ppm, anddoublet of doublets at δ 7.44 ppm due to 5-bromo-2-hydroxybenzyl protons. The chemical shifts of the pyridyl protons appeared as two doublets at δ 7.86 and 8.81 ppm. The chemical shifts of the azomethine (N=CH) proton appeared as singlet at δ 8.66 ppm. The chemical

shifts of the hydroxy (-OH) and amide (NHCO) protons appear as a singlet at 11.15 and 12.37 ppm, respectively (Fig. S2). The $^{13}C$ NMR spectra of the title compound showed the chemical shifts of C=O and C-OH are at 160.96 and 155.94 ppm, respectively. The signals at 145.87 ppm are clearly assigned for azomethine group chemical shifts C=N. The signals at 121.00, 139.36 and 149.84 ppm are assigned for pyridyl carbons, while that the aromatic carbon chemical shifts of the compound occurred in the range of 110.03-133.36 ppm (Fig. S3).

### 3.4. ESI-MS study

The ESI-MS spectra show molecular ion peaks with m/z values 320.3 and 322.3 correspond to the molecular weight $[M+H]^+$. The m/z value 342.2 and 344.2 correspond to the sodiated molecular ion peak $[M+Na]^+$. These values are in good agreement with the proposed composition for the title molecule (Fig. S4).

### 3.5. Hirshfeld surfaces Analysis

The Hirshfeld surfaces calculated for the crystal structure of **2** in accord with the established procedures [54] provide an additional insight on the influence of weak intermolecular interactions on its molecular packing. In addition to broad and bright-red spots near amino-H atom H2N and pyridine-N atom N3 recognizing donor and acceptor of potential N-H…N hydrogen bond respectively on the Hirshfeld surfaces mapped over $d_{norm}$ in - 0.151 to + 1.197 arbitrary unit range (Fig. S5), the presences of diminutive and faint-red spots on the surface characterize the weak intermolecular interactions in the crystal. In the crystal packing of (**2**) the effect of short interatomic Br…O/O…Br and C…H/H…C contacts (Table S1) are viewed as the diminutive-red spots whereas the presence of weak intermolecular C-H…O and short interatomic C-C contacts with the faint-red spots (Fig. S5). The donors and acceptors of intermolecular interactions are also viewed as the blue and red regions on Hirshfeld surfaces mapped over electrostatic potential in -0.113 to +0. 153 a.u ranges around the respective atoms corresponding to positive and negative potentials (Fig. S6). The donors and acceptors of intermolecular C-H...π and its reciprocal i.e. π…H-C contact for **2**, influential on the packing are also illustrated through black-dotted lines joining blue-bump and light red-concave regions around them on the shape-index mapped Hirshfeld surfaces in Fig. 4a. The presence of π-π stacking interactions is illustrated through red-dotted lines in Fig. 4b.

The overall two dimensional fingerprint plot for **2**, Fig. 5a, and those delineated into H...H, O…H/H…O, N…H/H…N, C…C, C...H/H...C, Br...H/H...Br and Br...O/O…Br contacts [55] is illustrated in Fig. 5b-e, respectively. The quantitative summary of percentage contribution

from different interatomic contacts to the hirshfeld surfaces of **2** are summarized in Table S2. The pair of jaws-like peaks at de + di ~ 2.2 Å in fingerprint plot delineated into H...H contacts (Fig. 5b) indicate the presence of such short interatomic contact (Table S1) between methylene-H7and pyridyl-H11 atoms. The pair of long and thin spikes at de + di ~ 2.7 Å in the fingerprint plot delineated into N...H/H...N contacts in Fig. 5d had resulted are due to the formation of significant intermolecular N-H…N hydrogen bond. The effect of weak intermolecular C-H…O contact in the crystal structure of **2** is also evident as the pair of spikes having tips at de + di ~ 2.5 Å in the finger print delineated into O…H/H…O contacts, Fig. 5c, through such short interatomic contacts (Table S1). The presence of intermolecular of π-π stacking in the crystals of **2** is justified from the arrow-like distribution of points with the greater density around de = di ~ 1.8 Å in the fingerprint delineated into C…C contacts (Fig. 4e). The fingerprint plot delineated into C...H/H...C contacts (Fig. 5f) characterize short interatomic C…H/H…C contact and intermolecular C-H...π contact with the pairs of tips at de + di ~ 2.7 Å and ~ 2.8 Å respectively. The bromine substituent at phenol ring forms short interatomic contacts with pyridyl hydrogen-H13 and carbonyl oxygen-O2 showing forceps-like and needle shaped tips at de + di ~ 2.9 Å and at de + di ~ 3.1 Å with the asymmetric distribution of points in the respective delineated fingerprint plots (Fig. 5g, 5h). The small contributions from other interatomic contacts to the Hirshfeld surfaces summarized in Table S2 have negligible effects on the crystal packing.

The pairwise interaction energies between the molecules within the crystal are calculated by summing up four energy components comprising electrostatic ($E_{ele}$), polarization ($E_{pol}$), dispersion ($E_{dis}$) and exchange - repulsion ($E_{rep}$) [56]. These energies were obtained by using the wave function calculated at HF/STO-3G level theory. The quantitative summary of the strength and nature of intermolecular interactions in the crystals of **2** is illustrated in Table 4. It is observed from the interaction energies calculated between the reference molecule and the inversion related molecule at –x, -y, -z that maximum energy from dispersive components had resulted greatest total energy of interaction in the formation of π-π stacking. From interaction energies calculated between the reference molecule and the molecule at -1/2+x,-1/2-y, 1/2+z, the electrostatic energy component is significant due to intermolecular N-H...N hydrogen bond whereas dispersive components are dominant due to short interatomic contacts related with the same molecules. The intermolecular C-H…O interaction between phenyl-C12 and hydroxyl-O1 is stronger compared to intermolecular C-H…π contacts. The other short

interatomic contacts involving bromine Br1 as summarized in Table 4 have small interaction energies due to greater contribution from repulsive components.

The magnitudes of intermolecular energies are represented graphically in the energy frameworks for both the analogues down-c axis in Fig. 6. Here the supramolecular architecture of crystals is viewed through the cylinders joining centroids of molecular pairs by using red, green and blue colour codes for the components $E_{ele}$, $E_{disp}$ and $E_{tot}$ respectively. The radius of the cylinder is proportional to the magnitude of interaction energy which is adjusted to same scale factor 5 kJ $mol^{-1}$ within 4 × 4 × 4 unit cells. From the energy frameworks illustrated in the supramolecular associations viewed down-c axis in Fig. 6 for the crystal structure of **2**, it is clearly seen that the electrostatic and dispersive energy components are dominant between different groups of atoms.

### 3.6. Molecular electrostatic potential (MEP)

Electrostatic potential is a very important property because it provides us much information on the chemical reactivity of the studied compound especial to describe intermolecular interactions. Based on a color code to detect and display regions and molecular properties of the electrostatic potential. The blue color indicates positive values, red for negative values and green indicate the neutral zone. The blue color indicates the strongest attraction and the red indicates the strongest repulsion. It is very useful for the qualitative interpretation of electrophilic and nucleophilic reactions and hydrogen bond interactions. The total electron density surface mapped with electrostatic potential of compound **2** constructed using B3LYP/6-311++G(d,p) level is shown in Fig. 7. The regions of negative potentials (excess in electrons) are associated with the hydrogen atoms especial that which is linked the nitrogen atoms whereas the regions of positive potentials (deficient in electrons) are associated with the oxygen and the bromine atoms. Indeed the electrophilic and nucleophilic sites confirm well the existence of N-H···N and C-H···O hydrogen bonds interactions between the entities of our compound and explain their important role in the stabilization of the crystal.

### 3.7. Frontier molecular orbital analysis

The electronic properties and the chemical reactivity behaviors of the chosen molecule have been performed via TD-DFT approach [57, 58]. The Highest Occupied Molecular Orbital (HOMO) and the Lowest Unoccupied Molecular Orbital (LUMO), called frontier molecular orbitals (FMOs), are the most important orbital in molecules. These two orbitals specify the manner in which the molecule interacts with species. The energy of the HOMO is linked to the ionization potential, while LUMO energy is linked to the electron affinity. The 3D plots of

the FMOs of the compound **2** are displayed in Fig. 8. The DFT calculated reactivity descriptors: energy band gap, ionization potential, electron affinity, chemical hardness, chemical softness, electronegativity, chemical potential, electrophilicity index and the maximum charge transfer index are determined in Table 5. Results reveal the energy level of the HOMO orbital is equal to -6.395 eV and the energy level of the LUMO orbital is equal to -2.575 eV, which gives an energy gap about -3.820 eV. This gap energy describes well the molecular chemical reactivity [59, 60]. All the parameters given in the table 7 are related to the energies of HOMO and LUMO orbitals by the following relations: the ionization potential $I = -E_{HOMO}$, the electron affinity $A= -E_{LUMO}$ and the electronic chemical potential $\mu= 1/2(I+A)$. These parameters are equal to -3.820, 6.395 and -4.485 eV, respectively. The chemical hardness ($\eta$) can be estimated as $E_{LUMO}–E_{HOMO}= (I−A)$ and found about 1.910 eV. Additionally, our molecule has a chemical softness ($\zeta = 1/2\eta$) equal to 0.262 $eV^{-1}$. The Electronegativity ($\chi = (I+A)/2$) is computed based on the HOMO and LUMO energies and found to be 4.485 eV. Also, the compound **2** has an electrophilicity index $\omega = \mu^2/2\eta$ about 10.534 eV. Finally, the maximum charge transfer index ($\Delta N_{max}= –\mu/\eta$) has been calculated and found to be 2.349.

### 3.8. Thermodynamic properties

The thermodynamic functions such as enthalpy change (H), entropies (S) and heat capacity at a constant pressure (Cp) were determined for the title compound using B3LYP/6-311++G(d,p) at different temperatures 100-1000K and as observed in Fig. 9 and Table 6**.** It can be shown that these thermodynamic functions increase with temperature as predicted that the molecular vibrational intensities change with rise of temperature. The correlation equations between heat capacities, entropies, enthalpy changes and temperatures were fitted by quadratic formulas, and the corresponding fitting factors (R2) for these thermodynamic properties are 0.99961, 0.99997 and 0.99951, respectively. The corresponding fitting equations are as follow:

$$C_p = 19.69087+0.96165T -4.27323 \times 10^{-4} T^2 \ (R^2= 0.99961)$$

$$S = 275.35652+ 1.05962T -2.63098 \times 10^{-4} T^2 \ (R^2= 0.99997)$$

$$H = -12.72168 +0.1309T + 2.45152 \times 10^{-4} T^2 \ (R^2= 0.99951)$$

These equations above will be helpful for deepened studies of the title compound. We note that all thermodynamic calculations were done in the gas phase and could not be used in solution.

### 3.9. Anti-diabetic activity

The antidiabetic activity of the title compound has been systematically evaluated against two enzymes at different concentration. The α-glucosidase and α-amylase inhibition capacity of the compound under investigation was fixed. Table 7 illustrates the $IC_{50}$ values of the in vitro antidiabetic profile of the title molecule, compared to acarbose as reference drug. *In vitro* study on the inhibition of α-glucosidase shows that compound **2** has significant activity with an $IC_{50}$ value of 280.45 ± 1.55 µM. This value is 2.85 and 22.08-fold lower than those of acarbose ($IC_{50}$ = 98.12 µM) and resveratrol ($IC_{50}$ = 12.70 µM) [61, 62], well-known as α-glucosidase inhibitors, respectively. The results of the α-amylase test reveal that the compound **2** has a good inhibitory activity with an $IC_{50}$ value of 135.02 ± 1.43 µM, compared with that of the reference acarbose ($IC_{50}$ = 2.29 ± 0.21 µM) (Table 7).

In summarize, building on the results obtained from the comparison performed between **2** and acarbose on front of α-glucosidase and α-amylase enzymes, the title compound might be used as potent α- glucosidase inhibitor.

### 3.10. Molecular docking

The prediction of the ligand-protein conformation was performed using iGEMDOCK program, in order to confirm the potency of inhibition activities of (*E*)-*N'*-(5-bromo-2-hydroxybenzylidene)isonicotinohydrazide (**2**) compound against Alpha-glucosidase GSJ and *α*-amylase enzymes. Also to give vision into the mechanism of action of potential antidiabetic drugs."α-glucosidase GSJ" receptor represents an extremely common enzyme, whose role appears in anti-bacterial defenses and the breakdown of complex carbohydrates. Several diseases are linked to deficiencies of this protein, which can lead to problems during development and sometimes can lead to death. The second receptor "*α*-amylase"is a digestive enzyme; it is a constituent of saliva and pancreatic juice. This enzyme is linked to bacteria that can ferment the glucose that it produces into organic acid. In this work, docking analysis was performed to explore the binding mechanism of the molecule **2** to the *α*-glucosidase and *α*-amylase enzymes to allow the design of new **2**-based 1CLV/2ZE0 inhibitors.

In Table 8, we present the docking energies and their distributions (VDW, H-bond, electronic interactions and Averconpair). The best docked conformation of the ligand **2** in the binding sites of 2ZE0 and 1CLV proteins and their 2D interactions are illustrated in Fig. 10, respectively. Docking calculations predicted good total energy score of the title compound with the selected target. **2**-2ZE0 is more stable than **2**-1CLV complexes since it has the best

inhibitory impact whose their total energy score equal to -108.68 Kcal/mol, while it is a little weak for the **2**-1CLV complex (E=-94.82 Kcal/mol). Docking results reveal that the main interaction forces are H-bond and VDW interaction (as shown in Table 8). The two complexes have very nearby VDW interactions, but **2**-2ZE0 take the strongest VDW interaction which is equal to -96.447 kcal/mol. Likewise, this complex presents the strongest Hydrogen bonding interaction (-12.233 kcal/mol). While **2**-1CLV complexe have the highest AverConPair (25.52 kcal/mol). In addition, the 2 dimensional representations demonstrate the interactions existing between our molecule and the amino acid of the selected proteins. For 2ZE0-**2**, the VDW interactions were observed between **2** and A:LYS:2, A:ARG:315, A:GLY:270, A:ASN:273 and A:TRP:317 amino residues. The A:GLU:271 and A:GLY:316 form two H-bonds with oxygen atoms (O2 and O3) of 5-bromo-2-hydroxybenzyl ring and acylhydrazone group, respectively. Then the pyridine and 5-bromo-2-hydroxybenzyl ring form pi-donor hydrogen bonds with A:GLU:272 and A:ASN:314 residues. Concerning 1CLV protein, our molecule interact with the following amino acids: A:ASN:468, A:GLN:35, A:TYR:368, A:GLY:369, A:ARG:365, A:LEU:432, A:HIS:466, A:GLY:36 and A:GLY:9 creating nine Van der Waals interactions. The carbon atom C16 of acylhydrazone group participate with A:GLY:372 in carbon hydrogen bond. In the other hand, there are also other types of contacts existing among the both complexes like; pi-anion, pi-cation, Amide-pi stacked.... In order to better understand the binding of these complexes, the hydrogen bonding interactions were also investigated and depicted in Fig. S7. This latter show that, the 5-bromo-2-hydroxybenzyl ring participate as an electron donor-acceptor in the same time for the both complexes. Whereas, the pyridine ring and acylhydrazone (-CO-NH-N=CH-) group are involved like electron acceptor in **2**-2ZE0 and **2**-1CLV. The main conclusion can be drawn from these results is that the title molecule promotes inhibition of enzyme activity, i.e. it contributes greatly and effectively to the treatment of diabetic diseases.

## 4. Conclusions

In summary, new crystal, (*E*)-*N'*-(5-bromo-2-hydroxybenzylidene)isonicotinohydrazide (**2**) has been synthesized and characterized by FT-IR, $^{1}$H- and $^{13}$C-NMR, ESI-MS and the (*E*)-configuration of azomethine (N=CH) group was comfirmed using single-crystal X-ray diffraction analysis. Based on the optimized structure analysis, the theoretical results (DFT/B3LYP) are in agreement with the experimental ones. Intra-molecular interaction of the compound was investigated via Hirshfeld surface analysis. The compound is a good non-linear optical material candidate and the most reactive site of the compound is around the

nitrogen atoms (electrophilic attack region), based on the MEP surface. The in vitro antidiabetic activity of the title compound was evaluated against α-glucosidase and α-amylase enzymes, and compared to acarbose building on $IC_{50}$ value demonstrating an important inhibitory effect on front of the both enzymes especially for α-glucosidase. A molecular docking studies showed that the **2**-*α*-glucosidase GSJ complex is more stable than **2**-*α*-amylase complex, since it has the best inhibitory impact whose their total energy score equal to -108.68 Kcal/mol. Docking results reveal that the main interaction forces are H-bond and van der Waals interactions.

**Conflicts of Interest**

The authors declare no conflict of interest.

**Acknowledgments**

The authors extend their appreciation to the Deanship of Scientific Research at King Khalid University for its funding this prolific research group no. (R.G.P. 2/115/41). This work was also supported by PPR2-MESRSFC-CNRST-P10 project (Morocco) as well as the UM5R.

**Supplementary crystallographic data:** CCDC 1836620 for **2** contain the supplementary crystallographic data for these compounds, and can be obtained free of charge from the Cambridge Crystallographic Data Centre via www.ccdc.cam.ac.uk/data_request/cif.

**Supporting Information Available: Figures S1-S7, Tables S1 and S2**.

**References**

[1] A. D. Deshpande, M. Harris-Hayes, M. Schootman. Epidemiology of diabetes and diabetes-related complications. Phys. Ther. 88 (2008) 1254-1264.

[2] Joshi, S. R., Standl, E., Tong, N., Shah, P., Kalra, S., & Rathod, R. Therapeutic potential of α-glucosidase inhibitors in type 2 diabetes mellitus: an evidence-based review. Expert. Opin. Pharmaco. 16 (2015) 1959-1981.

[3] Mahmood, N. A review of α-amylase inhibitors on weight loss and glycemic control in pathological state such as obesity and diabetes. Comp. Clin. Path. 25 (2016) 1253-1264.

[4] R. Rafique, K. M. Khan, S. Chigurupati, A.,Wadood, A. U. Rehman, A. Karunanidhi, Al-Rashida, M. Synthesis of new indazole based dual inhibitors of α-glucosidase and α-amylase enzymes, their in vitro, in silico and kinetics studies. Bioorg. Chem. 94 (2020) 103195.

[5] P. Singh, S. Mothilal, N. Kerru, A. Singh-Pillay, L. Gummidi, O. L. Erukainure, M. S. Islam. Comparative α-glucosidase and α-amylase inhibition studies of rhodanine–pyrazole conjugates and their simple rhodanine analogues. Med. Chem. Res. 28 (2019) 143-159.

[6] S. Thota, D. A. Rodrigues, P. D. S. M. Pinheiro, L. M. Lima, C. A. Fraga, E. Barreiro.N-Acylhydrazones as drugs. Bioorg. Med. Chem. Lett. 28 (2018) 2797-2806.

[7] R. D. C.Maia, R.Tesch, C. A. M. Fraga. Acylhydrazone derivatives: a patent review. Expert. Opin. Ther. Patents. 24 (2014) 1161-1170.

[8] K. Karrouchi, S. Radi, M. Ansar, J. Taoufik, H. A. Ghabbour, Y. N. Mabkhot. Crystal structure of N′-(4-(dimethylamino)benzylidene)-5-phenyl-1H-pyrazole-3-carbohydrazide, C19H19N5O. Z. Kristallogr. NCS. 231(2016) 883-886.

[9] M. M. Andrade, M. T. Barros. Fast Synthesis of N-Acylhydrazones Employing a Microwave Assisted Neat Protocol. J. Comb. Chem. 12(2010) 245-247.

[10] K. Karrouchi, S. Radi, M. Ansar, J. Taoufik, H. A. Ghabbour, Y. N. Mabkhot. Crystal structure of N′-(4-nitrobenzylidene)-5-phenyl-1H-pyrazole-3-carbohydrazide, C17H13N5O3. Z. Kristallogr. NCS. 231(2016)839-841.

[11] D. Hean, J. P. Michael, A. Lemmerer.Supramolecular packing and polymorph screening of N-isonicotinoyl arylketone hydrazones with phenol and amino modifications. J. Mol. Struct. 1157 (2018) 693-707.

[12] J. B. He, L. L. Feng, J. Li, R. J. Tao, Y. L. Ren, J. Wan, H. W. He. Design, synthesis and molecular modeling of novel N-acylhydrazone derivatives as pyruvate dehydrogenase complex E1 inhibitors. Bioorg. Med. Chem. 22(2014)89-94.

[13] P. Hernández, M. Cabrera, M. L. Lavaggi, L. Celano, I. Tiscornia, T. R. da Costa, L. Thomson, M. Bollati-Fogolin, A. L. P. Miranda, L. M. Lima, E. J. Barreiro, M. Gonzalez, H. Cerecetto.Discovery of new orally effective analgesic and anti-inflammatory hybrid furoxanyl N-acylhydrazone derivatives. Bioorg. Med. Chem. 20(2012) 2158-2171.

[14] N. A. Khalil, E. M. Ahmed, K. O.Mohamed, S. A. B. Zaitone. Synthesis of new nicotinic acid derivatives and their evaluation as analgesic and anti-inflammatory agents. Chem. Pharm. Bull. 61(2013)933-940.

[15] J. R. Burgeson, D. N. Gharaibeh, A. L. Moore, R. A. Larson, S. M. Amberg, B. Tove'C, E. H.Dennis, D. Dai. Lead optimization of an acylhydrazone scaffold possessing antiviral activity against Lassa virus. Bioorg.Med. Chem. Lett. 23(2013)5840-5843.

[16] K. Karrouchi, S. Fettach, S. Radi, J. Taoufik, Y. N. Mabkhot, S. Alterary, My E. A Faouzi, M. Ansar. Synthesis, Characterization, Free-radical Scavenging Capacity and Antioxidant Activity of Novel Series of Hydrazone, 1, 3, 4-oxadiazole and 1, 2, 4-triazole Derived from 3, 5-dimethyl-1H-pyrazole. Lett. Drug. Des. Discov. 16 (2019) 712-720.

[17] R. K.Singh, A. K.Singh, S.Siddiqui, M.Arshad,A. Jafri. Synthesis, molecular structure, spectral analysis and cytotoxic activity of two new aroylhydrazones. J. Mol. Struct. 1135(2017)82-97.

[18] A. G.Silva, G.Zapata-Sudo, A. E.Kummerle, C. A.Fraga, E. J.Barreiro,R. T. Sudo. Synthesis and vasodilatory activity of new N-acylhydrazone derivatives, designed as LASSBio-294 analogues. Bioorg. Med. Chem. 13(2005)3431-3437.

[19] A. C.Cunha, J. M.Figueiredo, J. L. Tributino, A. L. Miranda, H. C.Castro, R. B. Zingali,E. J. Barreiro. Antiplatelet properties of novel N-substituted-phenyl-1, 2, 3-triazole-4-acylhydrazone derivatives. Bioorg. Med. Chem. 11(2003)2051-2059.

[20] N. C. Romeiro, G. Aguirre, P. Hernández, M. González, H. Cerecetto, I. Aldana, L. M. Lima. Synthesis, trypanocidal activity and docking studies of novel quinoxaline-N-acylhydrazones, designed as cruzain inhibitors candidates. Bioorg. Med. Chem. 17(2009)641-652.

[21] K. Karrouchi, E. Yousfi, N. Sebbar, Y. Ramli, J. Taoufik, Y. Ouzidan, M. Ansar, Y. Mabkhot, H. Ghabbour, S. Radi. New Pyrazole-Hydrazone Derivatives: X-ray Analysis, Molecular Structure Investigation via Density Functional Theory (DFT) and Their High In-Situ Catecholase Activity. Int J Mol Sci. 2017; 18:2215.

[22] M. Mangalam, C. S. A.Selvan, C. Sankar. Synthesis, stereochemical, structural, and biological studies of a series of N′-(2r, 4c-diaryl-3-azabicyclo [3.3. 1] nonan-9-ylidene) pyrazine-2-carbohydrazides. J. Mol. Struct.1129(2017)305-312.

[23] R. R.Pillai, K.Karrouchi, S.Fettach, S.Armaković, S. J.Armaković, Y.Brik, J.Taoufik, S.Radi, M. E. A.Faouzi, M.Ansar, Synthesis, spectroscopic characterization, reactive properties by DFT calculations, molecular dynamics simulations and biological

evaluation of Schiff bases tethered 1, 2, 4-triazole and pyrazole rings. J. Mol. Struct.1177(2019)47-54.

[24] O. Noureddine, S. Gatfaoui, S.A. Brandán, H. Marouani, N. Issaoui, Structural, docking and spectroscopic studies of a new piperazine derivative, 1-Phenylpiperazine-1,4-diium-bis (hydrogen sulfate), J. Mol. Struct. 1202 (2020) 127351.

[25] M.A. Iramain, M.V. Castillo, L. Davies, E. María, M.E. Manzur, S.A. Brandán. Structural and SQMFF study of potent insecticide 4,4-DDT combining the FT-IR and FT-Raman spectra with DFT calculations. J. Mol. Struct. 1199 (2020) 126964.

[26] S. Tighadouini, R. Benabbes, M. Tillard, D. Eddike, K. Haboubi, K. Karrouchi, S. Radi. Synthesis, crystal structure, DFT studies and biological activity of (Z)-3-(3-bromophenyl)-1-(1, 5-dimethyl-1 H-pyrazol-3-yl)-3-hydroxyprop-2-en-1-one. Chem. Cent. J. 12(1) (2018) 122.

[27] O. Noureddine, S. Gatfaoui, S.A. Brandan, A. Sagaama, H. Marouani, N. Issaoui, Experimental and DFT studies on the molecular structure, spectroscopic properties, and molecular docking of 4-phenylpiperazine-1-ium dihydrogen phosphate, J Mol. Struct. 1207 (2020) 127762.

[28] J. Kausteklis, V. Aleksa, M.A. Iramain, S.A. Brandán. DFT study and vibrational assignment of 1-Butyl-3-methylimidazolium trifluoromethanesulfonate ionic liquid by using the FT-Raman spectrum. J. Mol. Struct. 1175 (2019) 663-676.

[29] Y. Bouzian, K. Karrouchi, Y. Sert, C. H. Lai, L. Mahi, N. H. Ahabchane,. A. Talbaoui, J. T. Mague, E. M. Essassi. Synthesis, spectroscopic characterization, crystal structure, DFT, molecular docking and in vitro antibacterial potential of novel quinoline derivatives. J. Mol. Struct. 1209 (2020). 127940.

[30] N. Issaoui, , H. Ghalla, , F. Bardak, M. Karabacak, N. A. Dlala, H. T. Flakus, & B. Oujia, Combined experimental and theoretical studies on the molecular structures, spectroscopy, and inhibitor activity of 3-(2-thienyl) acrylic acid through AIM, NBO, FT-IR, FT-Raman, UV and HOMO-LUMO analyses, and molecular docking. Journal of Molecular Structure, 1130 (2017) 659-668.

[31] K. Karrouchi, S. Radi, J. Taoufik, H. A. Ghabbour, Y. N. Mabkhot. Crystal structure of N′-(4-(dimethylamino) benzylidene)-5-phenyl-1H-pyrazole-3-carbohydrazide, C19H19N5O. Z. Kristallogr. NCS. 231 (2016) 883-886.

[32] K. Karrouchi, S. Radi, J. Taoufik, H. A. Ghabbour, Y. N. Mabkhot. Crystal structure of N′-(4-methoxybenzylidene)-5-phenyl-1H-pyrazole-3-carbohydrazide, C18H16N4O2. Z. Kristallogr. NCS. 231 (2016) 835-837.

[33] K. Karrouchi, S. Radi, J. Taoufik, H. A. Ghabbour, Y. N. Mabkhot. Crystal structure of N′-(4-nitrobenzylidene)-5-phenyl-1H-pyrazole-3-carbohydrazide, C17H13N5O3. Z. Kristallogr. NCS. 231 (2016) 839-841.

[34] Sheldrick, G.M. A short history of SHELX. ActaCrystallogr. 64(2008) 112–122.

[35] Sheldrick, G.M. Program SHELXTL97; Siemens Analytical X-ray Instruments, Inc.: Madison, WI, USA, 1997.

[36] Frisch MJ, Trucks GW, Schlegel HB, Scuseria GE, Robb MA, Cheeseman JR, Scalmani G, Barone V, Mennucci B, Petersson GA, Nakatsuji H, Caricato M, Li X, Hratchian HP, Izmaylov AF, Bloino J, Zheng G, Sonnenberg JL, Hada M, Ehara M, Toyota K, Fukuda R, Hasegawa J, Ishida M, Nakajima T, Honda Y, Kitao O, Nakai H, Vreven T, Montgomery Jr JA, Peralta JE, Ogliaro F, Bearpark M, Heyd JJ, Brothers E, Kudin KN, Staroverov VN, Keith T, Kobayashi R, Normand J, Raghavachari K, Rendell A, Burant JC, Iyengar SS, Tomasi J, Cossi M, Rega N, Millam JM, Klene M, Knox JE, Cross JB, Bakken V, Adamo C, Jaramillo J, Gomperts R, Stratmann RE, Yazyev O, Austin AJ, Cammi R, Pomelli C, Ochterski JW, Martin RL, Morokuma K, Zakrzewski VG, Voth GA, Salvador P, Dannenberg JJ, Dapprich S, Daniels AD, Farkas O, Foresman JB, Ortiz JV, Cioslowski J, Fox DJ (2013) GAUSSIAN 09, revision E.01. Gaussian, Inc, Wallingford.

[37] R. Dennington, T. Keith, J. Millam, *GaussView, Version 5*, Semichem Inc., Shawnee Mission, KS, 2009.

[38] A.D. Becke. Density-functional thermochemistry. I. The effect of the exchange-only gradient correction. J. Chem. Phys. 96 (1992) 2155–2160.

[39] C. Lee, W. Yang, R.G. Parr,Density-functional exchange-energy approximation with correct asymptotic behaviour. Phys. Rev. B**.** 37 (1988) 785–789.

[40] J.M. Yang, C.C. Chen, GEMDOCK: a generic evolutionary method for molecular docking, Proteins Struct. Funct. Bioinforma. 55 (2004) 288-304.

[41] D.S. Visualizer, Accelrys software inc. Discovery Studio Visualizer 2 (2005).

[42]T. Shirai, V. S. Hung, K. Morinaka, T. Kobayashi, S. Ito. Crystal structure of GH13 α-glucosidase GSJ from one of the deepest sea bacteria. Proteins: Struct.,Funct., Bioinf. 73 (2008) 126-133.

[43] P. J. B. Pereira, V. Lozanov, A. Patthy, R. Huber, W. Bode, S. Pongor, S. Strobl. Specific inhibition of insect α-amylases: yellow meal worm α-amylase in complex with the Amaranth α-amylase inhibitor at 2.0 Å resolution. Structure. 7 (1999) 1079-1088.

[44] Fettach, S.; Mrabti, H. N.; Sayah, K.; Bouyahya, A.; Salhi, N.; Cherrah, Y.; El Abbes, F. Phenolic content, acute toxicity of Ajugaiva extracts and assessment of their antioxidant and carbohydrate digestive enzyme inhibitory effects. S. Afr. J. Bot. 125, (2019) 381-385.

[45] K.Govindarasu, E.Kavitha, N.Sundaraganesan, M.Suresh, M. S. A. Padusha. Synthesis, structural and spectral analysis of (E)-N′-(4-Methoxybenzylidene) pyridine-3-carbohydrazide dihydrate by density functional theory. Spectrochim. Acta A. 135(2015) 1123-1136.

[46] L. V. de Freitas, C. C. da Silva, J. Ellena, L. A. S. Costa, N. A. Rey. Structural and vibrational study of 8-hydroxyquinoline-2-carboxaldehyde isonicotinoylhydrazone–A potential metal–protein attenuating compound (MPAC) for the treatment of Alzheimer's disease. Spectrochim. Acta A.116 (2013) 41-48.

[47] A. C. González-Baró, R. Pis-Diez, B. S. Parajón-Costa, N. A. Rey. Spectroscopic and theoretical study of the o-vanillin hydrazone of the mycobactericidal drug isoniazid. J. Mol. Struct. 1007 (2012) 95-101.

[48] T. Benković, A. Kenđel, J. Parlov-Vuković, D. Kontrec, V. Chiş, S. Miljanić, N. Galić. Aromatic hydrazones derived from nicotinic acid hydrazide as fluorimetric pH sensing molecules: Structural analysis by computational and spectroscopic methods in solid phase and in solution. Spectrochim. Acta. Part A. 190 (2018) 259-267.

[49] D. Michalska, D. C. Bieńko, A. J. Abkowicz-Bieńko, Z. Latajka. Density functional, Hartree− Fock, and MP2 studies on the vibrational spectrum of phenol. J. Phys. Chem. 100 (1996) 17786-17790.

[50] C. Arunagiri, A. G. Anitha, A. Subashini, S. Selvakumar. Synthesis, X-ray crystal structure, vibrational spectroscopy, DFT calculations, electronic properties and Hirshfeld analysis of (E)-4-Bromo-N'-(2, 4-dihydroxy-benzylidene) benzohydrazide. J. Mol. Struct. 1163 (2018) 368-378.

[51] S. R. Sheeja, N. A. Mangalam, M. P. Kurup, Y. S. Mary, K. Raju, H. T. Varghese, C. Y. Panicker. Vibrational spectroscopic studies and computational study of quinoline-2-carbaldehyde benzoyl hydrazone. J. Mol. Struct. 973 (2010) 36-46.

[52] P. Larkin. Infrared and Raman spectroscopy: principles and spectral interpretation. Elsevier, (2017).

[53] N. Galić, A. Dijanošić, D. Kontrec, S. Miljanić. Structural investigation of aroylhydrazones in dimethylsulphoxide/water mixtures. Spectrochim. Acta. Part A. 95 (2012) 347-353.

[54] S. L. Tan, M. M. Jotani, E. R. Tiekink. Utilizing Hirshfeld surface calculations, non-covalent interaction (NCI) plots and the calculation of interaction energies in the analysis of molecular packing. ActaCryst. E75 (2019) 308–318.

[55] J. J. McKinnon, D.Jayatilaka, M. A.Spackman. Towards quantitative analysis of intermolecular interactions with Hirshfeldsurfaces.Chem. Commun.(37)(2007) 3814–3816.

[56] M. J. Turner, J. J. McKinnon, S. K. Wolff, D. J.Grimwood, P. R.Spackman, D. Jayatilaka, M. A. Spackman. CrystalExplorer17. University of Western Australia (2017). http://hirshfeldsurface.net.

[57] Gatfaoui, S., Issaoui Noureddine, Roisnel, T., Marouani, H., A proton transfer compound template phenylethylamine: Synthesis, a collective experimental and theoretical investigations, J. Mol. Struct. 1191, (2019) 183-196.

[58] R.E. Stratmann, G.E. Scuseria, M.J. Frisch, An efficient implementation of timedependent density-functional theory for the calculation of excitation energies of large molecules, J. Chem. Phys. 109 (1998) 8218-8224.

[59] N. Issaoui, H. Ghalla, S. A. Brandán, F. Bardak, H. T.Flakus, A. Atac, B.Oujia, Experimental FTIR and FT-Raman and theoretical studies on the molecular structures of monomer and dimer of 3-thiopheneacrylic acid. J. Mol. Struct. 1135 (2017) 209-221.

[60] A. Rauk, Orbital Interaction Theory of Organic Chemistry, second ed., WileyInterscience, New York, 2001.

[61] D. Avcı, S. Altürk, F. Sönmez, Ö. Tamer, A. Başoğlu, Y. Atalay, B. Z. Kurt, D. Öztürk, N. Dege. A new dinuclear copper (II) complex of 2, 5–Furandicarboxyclic acid with 4 (5)-Methylimidazole as a high potential α-glucosidase inhibitor: Synthesis, Crystal structure, Cytotoxicity study, and TD/DFT calculations. Appl. Organomet. Chem. 33 (2019) e4725.

[62] D. Avcı, S. Altürk, F. Sönmez, Ö. Tamer, A. Başoğlu, Y. Atalay, B. Z. Kurt, N. Dege. Novel Cu (II), Co (II) and Zn (II) metal complexes with mixed-ligand: Synthesis, crystal structure, α-glucosidase inhibition, DFT calculations, and molecular docking. J. Mol. Struct. 1197 (2019) 645-655.

**Caption Figures**

**Figure 1.** The molecular structure of **2** showing the atomic labeling scheme and displacement ellipsoids at 50 % probability level.

**Figure 2.** The optimized geometry of compound **2** using B3LYP/6-311++G(d,p) theory.

**Figure 3.** The FT-IR experimental spectrum of compound **2**.

**Figure 4.** Views of Hirshfeld surface about reference molecule of **2**, (a) mapped with the shape-index property highlighting C-H…π/π…H-C contacts, (b) mapped over electrostatic potential highlighting of π-π stacking interactions.

**Figure 5.** The full two-dimensional fingerprint plot for **2** and those delineated into H...H, O…H/H…O, N…H/H…N, C…C, C...H/H...C, Br...H/H...Br and Br...O/O…Br contacts.

**Figure 6.** The energy frameworks composed of (a) electrostatic potential force, (b) dispersion force and (c) totalenergy for cluster about a reference molecule of **2**. The energy frameworks were adjusted to the same scale factor of 80 with a cut-off value of 5 kJ mol−1 within 4 × 4 × 4 unit cells.

**Figure 7.** Calculated molecular electrostatic potential contour map of **2**.

**Figure 8.** Frontier's molecular orbital HOMOs-LUMOs plots of the title compound with B3LYP/6-311++G(d,p).

**Figure 9.** Variation of entropy (S), heat capacity (C) and enthalpy (H) with temperature for the title molecule.

**Figure 10.** The best docked poses of the ligand **2** in the proteins 2ZE0 (a) and 1CLV (b) and their 2D interactions.

**Table 1**

Crystal data and structure refinement for **(2).**

| **CCDC Deposition Number** | **1836620** |
|---|---|
| **Crystal data** | |
| Chemical formula | $C_{13}H_{10}BrN_3O_2$ |
| $M_r$ | 320.15 |
| Crystal system, space group | Monoclinic, $P2_1/n$ |
| Temperature (K) | 293 |
| $a$, $b$, $c$ (Å) | 8.5812 (5), 15.9004 (10), 9.3872 (6) |
| β (°) | 100.472 (2) |
| $V$ (Å$^3$) | 1259.50 (13) |
| $Z$ | 4 |
| Radiation type | Mo $K\alpha$ |
| μ (mm$^{-1}$) | 3.27 |
| Crystal size (mm) | 0.51 × 0.28 × 0.18 |
| **Data collection** | |
| Diffractometer | Bruker *APEX*-II CCD |
| Absorption correction | Multi-scan<br>*SADABS* Bruker 2014 |
| $T_{min}$, $T_{max}$ | 0.943, 0.987 |
| No. of measured, independent and observed [$I$> 2σ($I$)] reflections | 29233, 5059, 2488 |
| $R_{int}$ | 0.087 |
| $(\sin \theta/\lambda)_{max}$ (Å$^{-1}$) | 0.783 |
| **Refinement** | |
| $R[F^2> 2\sigma(F^2)]$, $wR(F^2)$, $S$ | 0.052, 0.110, 1.00 |
| No. of reflections | 5059 |
| No. of parameters | 180 |
| No. of restrains | 2 |
| No. H-atom treatments | H atoms treated by a mixture of independent and constrained refinement |
| $\Delta\rho_{max}$, $\Delta\rho_{min}$ (e Å$^{-3}$) | 0.44, −0.63 |

**Table 2**
Hydrogen-bond geometry (Å, °) for (**2**).

| *D*—H···*A* | *D*—H | *H*···*A* | *D*···*A* | *D*—H···*A* |
|---|---|---|---|---|
| O1—H1O···N1 | 0.829 (17) | 1.83 (2) | 2.581 (3) | 149(4) |
| N2—H2N···N3$^{i}$ | 0.830 (16) | 2.225 (17) | 3.039 (3) | 167 (2) |
| C5—H5···Cg1$^{ii}$ | 0.93 | 2.85 | 3.477 (3) | 126 |

Symmetry code:*(i)x+1/2, -y-1/2, z+1/2; (ii) –x+1/2, y+1/2, -z-1/2*

**Table 3**

Optimized bond lengths and bond angles (Å, °) parameters of compound **(2).**

| | Theo. | Exp. | Δ(Theor-Exp.) |
|---|---|---|---|
| **Bond lengths** | | | |
| C1-Br1 | 1.918 | 1.892 | 0.026 |
| O2-C8 | 1.342 | 1.205 | 0.109 |
| O2-H | 0.982 | 0.867 | 0.116 |
| C8=O2 | 1.212 | 1.205 | 0.008 |
| N1-N2 | 1.358 | 1.370 | -0.013 |
| N1=C7 | 1.286 | 1.275 | 0.011 |
| N1-H1O | 1.820 | 1.830 | 0.010 |
| N2-C8 | 1.385 | 1.357 | 0.028 |
| N2-H2N | 1.015 | 0.830 | 0.185 |
| N3-C12 | 1.338 | 1.335 | 0.003 |
| N3-C11 | 1.335 | 1.332 | 0.003 |
| C4-C5 | 1.400 | 1.387 | 0.014 |
| C4-C3 | 1.419 | 1.402 | 0.017 |
| C5-H5 | 1.083 | 0.930 | 0.153 |
| C5-C6 | 1.387 | 1.378 | 0.009 |
| C6-H6 | 1.083 | 0.930 | 0.152 |
| C6-C1 | 1.397 | 1.380 | 0.017 |
| C1-C2 | 1.382 | 1.374 | 0.008 |
| C2-H | 1.084 | 0.930 | 0.154 |
| C2-C3 | 1.408 | 1.391 | 0.016 |
| C3-C7 | 1.451 | 1.460 | -0.009 |
| C7-H7 | 1.096 | 0.930 | 0.167 |
| C8-C9 | 1.504 | 1.503 | 0.001 |
| C9-C13 | 1.396 | 1.392 | 0.004 |
| C9-C10 | 1.397 | 1.377 | 0.020 |
| C13-H13 | 1.083 | 0.930 | 0.153 |
| C13-C12 | 1.392 | 1.377 | 0.014 |
| C12-H12 | 1.086 | 0.930 | 0.156 |
| C11-H11 | 1.086 | 0.930 | 0.156 |
| C11-C10 | 1.394 | 1.379 | 0.015 |
| C10-H10 | 1.084 | 0.930 | 0.155 |
| **RMSD** | **0.090** | | |
| **Bond angles** | | | |
| C4-O1-H1O | 109.8 | 107.0 | 2.800 |
| N2-N1-C7 | 118.8 | 119.5 | -0.700 |
| N1-N2-C8 | 120.1 | 115.3 | 4.761 |
| N1-N2-H2N | 119.3 | 120.0 | -0.700 |
| C8-N2-H2N | 120.1 | 124.0 | -3.900 |
| C12-N3-C11 | 117.3 | 116.4 | 0.900 |
| O1-C4-C5 | 117.7 | 117.9 | -0.200 |
| O1-C4-C3 | 123.1 | 122.5 | 0.600 |
| C5-C4-C3 | 119.1 | 119.6 | -0.500 |
| C4-C5-H5 | 118.2 | 119.6 | -1.400 |
| C4-C5-C6 | 121.0 | 120.7 | 0.343 |
| C6-C5-H | 120.8 | 119.7 | 1.112 |
| C5-C6-H | 120.1 | 120.2 | -0.127 |
| C5-C6-C1 | 119.7 | 119.6 | 0.136 |
| C1-C6-H6 | 120.2 | 120.2 | -0.009 |
| Br1-C1-C6 | 119.7 | 119.8 | -0.118 |
| Br1-C1-C2 | 119.8 | 119.4 | 0.391 |
| C6-C1-C2 | 120.5 | 120.6 | -0.100 |
| C1-C2-H2 | 120.2 | 119.8 | 0.439 |
| C1-C2-C3 | 120.5 | 120.5 | 0.000 |
| C3-C2-H2 | 119.3 | 119.8 | -0.510 |

| | | | |
|---|---|---|---|
| C2-C3-C4 | 119.1 | 119.0 | 0.100 |
| C4-C3-C7 | 122.1 | 121.9 | 0.200 |
| C2-C3-C7 | 118.8 | 119.1 | -0.301 |
| N1-C7-C3 | 121.4 | 118.7 | 2.672 |
| N1-C7-H7 | 121.4 | 120.6 | 0.800 |
| C3-C7-H7 | 117.3 | 120.7 | -3.400 |
| O2-C8-N2 | 123.0 | 122.2 | 0.800 |
| O2-C8-C9 | 122.7 | 121.5 | 1.200 |
| N2-C8-C9 | 114.3 | 116.3 | -1.966 |
| C8-C9-C13 | 118.0 | 116.9 | 1.020 |
| C8-C9-C10 | 124.1 | 124.9 | -0.875 |
| C10-C9-C13 | 118.0 | 118.0 | 0.000 |
| C9-C13-H13 | 119.9 | 120.6 | -0.721 |
| C9-C13-C12 | 118.7 | 118.7 | 0.074 |
| C12-C13-H13 | 121.3 | 120.7 | 0.646 |
| N3-C12-C13 | 123.7 | 123.9 | -0.232 |
| N3-C12-H12 | 116.1 | 118.1 | -1.964 |
| C13-C12-H12 | 120.2 | 118.0 | 2.196 |
| N3-C11-H11 | 116.2 | 117.9 | -1.693 |
| N3-C11-C10 | 123.6 | 124.2 | -0.600 |
| C10-C11-H11 | 120.1 | 117.9 | 2.200 |
| C9-C10-C11 | 118.7 | 118.7 | 0.000 |
| C9-C10-H10 | 122.0 | 120.6 | 1.359 |
| C11-C10-H10 | 119.3 | 120.6 | -1.321 |
| **RMSD** | **0.197** | | |

**Table 4**

Summary of energies calculated for intermolecular interactions in (**2**) (kJ $mol^{-1}$).

| Contact | R(Å) | $E_{ele}$ | $E_{pol}$ | $E_{dis}$ | $E_{rep}$ | $E_{tot}$ |
|---|---|---|---|---|---|---|
| N2-H2N...N3 | 9.89 | -43.1 | -15.7 | -22.8 | 37.9 | -43.9 |
| H7...H11 | | | | | | |
| H7...C11 | | | | | | |
| Cg(C1-C6)…...Cg (C9-C11/N3/C12-C13) | 4.40 | -34.6 | -7.2 | -89.0 | 52.1 | -77.9 |
| C6…C12 | 9.31 | -5.8 | -1.2 | -19.7 | 12.5 | -14.3 |
| C5-H5…Cg (C9-C11/N3/C12-C13) | | | | | | |
| O1…H12 | 9.78 | -20.3 | -6.3 | -18.7 | 7.8 | -35.3 |
| Br1…H13 | 11.51 | -4.1 | -2.4 | -11.8 | 13.9 | -5.1 |
| Br1…O2 | | | | | | |

**Table 5**
Some global reactivity descriptors the computed for the title compound (**2**).

| **Parameters (eV)** | **Values** |
|---|---|
| $E_{LUMO}$ | -2.57555892 |
| $E_{HOMO}$ | -6.39467876 |
| Energy band gap $\lvert E_{HOMO}–E_{LUMO}\rvert$ | 3.81911984 |
| Ionization potential ($I = –E_{HOMO}$) | 6.39467876 |
| Electron affinity ($A = –E_{LUMO}$) | 2.57555892 |
| Chemical hardness ($\eta = (I–A)/2$) | 1.90955992 |
| Chemical softness ($\zeta = 1/2\eta$) | 0.261840435 |
| Electronegativity ($\chi = (I+A)/2$) | 4.48511884 |
| Chemical potential ($\mu = –(I+A)/2$) | -4.48511884 |
| Electrophilicity index $\omega = \mu^2/2\eta$ | 10.53451677 |
| Maximum charge transfer index ($\Delta N_{max.} = –\mu/\eta$) | 2.348770936 |

**Table 6**

Calculated thermodynamic properties for (**2**) with DFT/B3LYP/6-311++G(d,p).

| T (K) | S(J/mol.K) | Cp(J/mol.K) | H(kJ/mol) |
|---|---|---|---|
| 100 | 374.97 | 116.158 | 7.694 |
| 150 | 429.086 | 153.337 | 14.43 |
| 200 | 478.356 | 191.143 | 23.038 |
| 250 | 525.133 | 229.589 | 33.556 |
| 298.15 | 568.724 | 266.314 | 45.498 |
| 300 | 570.376 | 267.704 | 45.992 |
| 350 | 614.414 | 304.244 | 60.299 |
| 400 | 657.292 | 338.261 | 76.374 |
| 450 | 698.954 | 369.264 | 94.075 |
| 500 | 739.331 | 397.15 | 113.248 |
| 550 | 778.374 | 422.065 | 133.741 |
| 600 | 816.07 | 444.282 | 155.41 |
| 650 | 852.429 | 464.115 | 178.129 |
| 700 | 887.485 | 481.87 | 201.787 |
| 750 | 921.285 | 497.826 | 226.286 |
| 800 | 953.881 | 512.222 | 251.543 |
| 850 | 985.332 | 525.261 | 277.486 |
| 900 | 1015.696 | 537.112 | 304.05 |
| 950 | 1045.03 | 547.92 | 331.179 |
| 1000 | 1073.39 | 557.803 | 358.826 |

$C_p = 19.69087+0.96165T -4.27323 \times 10^{-4} T^2$ ($R^2$= 0.99961)

$S = 275.35652+ 1.05962T -2.63098 \times 10^{-4} T^2$ ($R^2$= 0.99997)

$H =-12.72168 +0.1309T + 2.45152 \times 10^{-4} T^2$ ($R^2$= 0.99951)

**Table 7**
Antidiabetic activity of **(2).**

| Compound | $IC_{50}$ (μM) | |
|---|---|---|
| | α-glucosidase | α-amylase |
| **2** | 280.45 ± 1.55 | 135.02 ± 1.43 |
| **Acarbose** | 98.12 ± 2.08 | 2.29 ± 0.21 |

**Table 8**

Energies of the protein-ligand obtained from molecular docking of **(2).**

| Target protein | Total energy | VDW | H-bond | Electronic | AverConPair |
|---|---|---|---|---|---|
| **2ZE0** | -108.680 | -96.447 | -12.233 | 0 | 23.360 |
| **1CLV** | -94.820 | -91.924 | -2.897 | 0 | 25.520 |

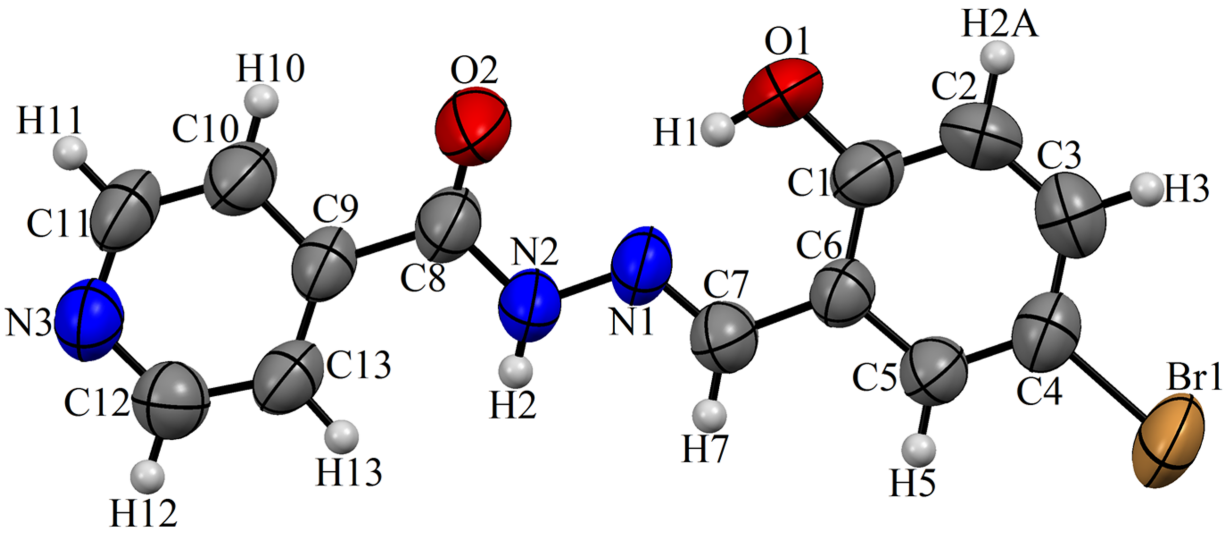

(a) 2ZE0-**2**


(b) 1CLV-**2**

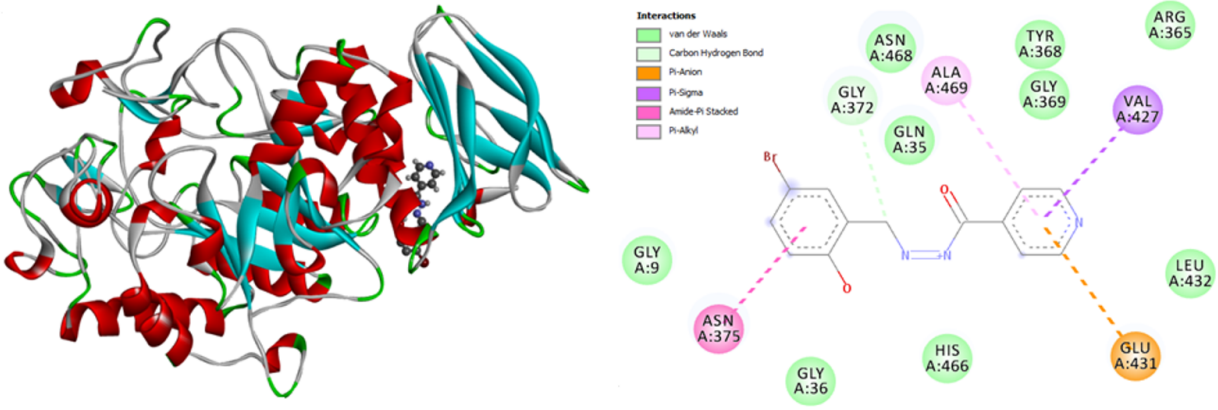

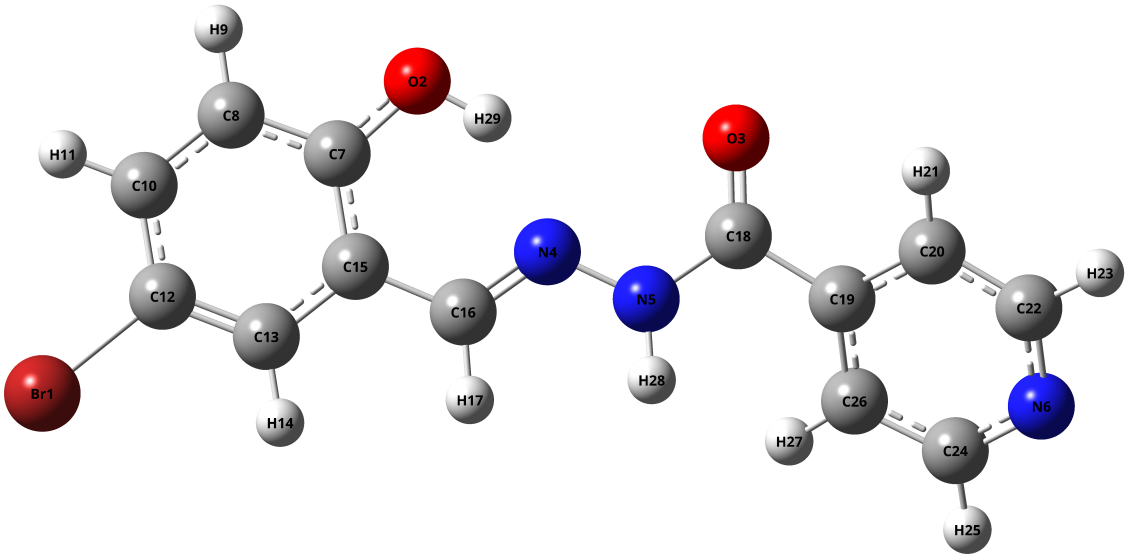

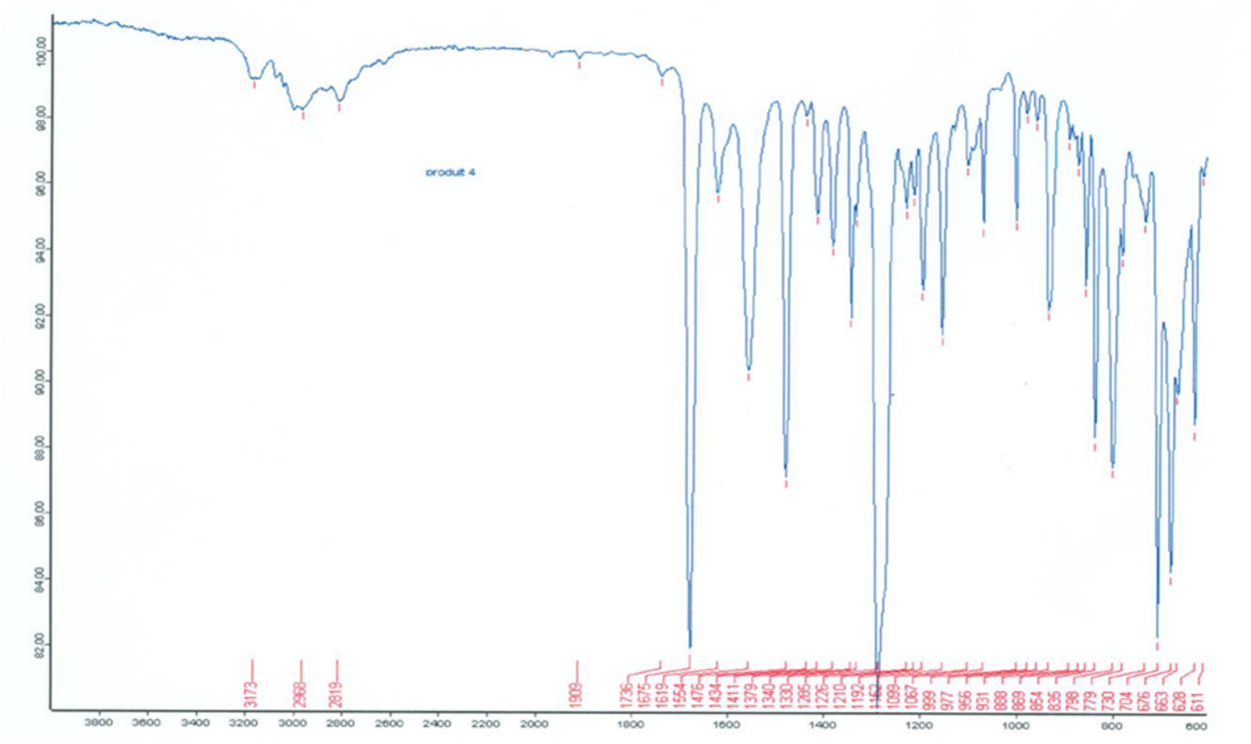

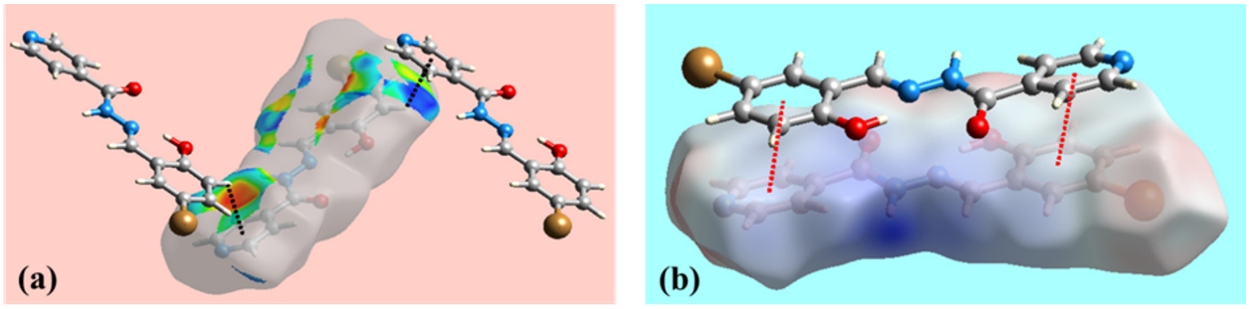

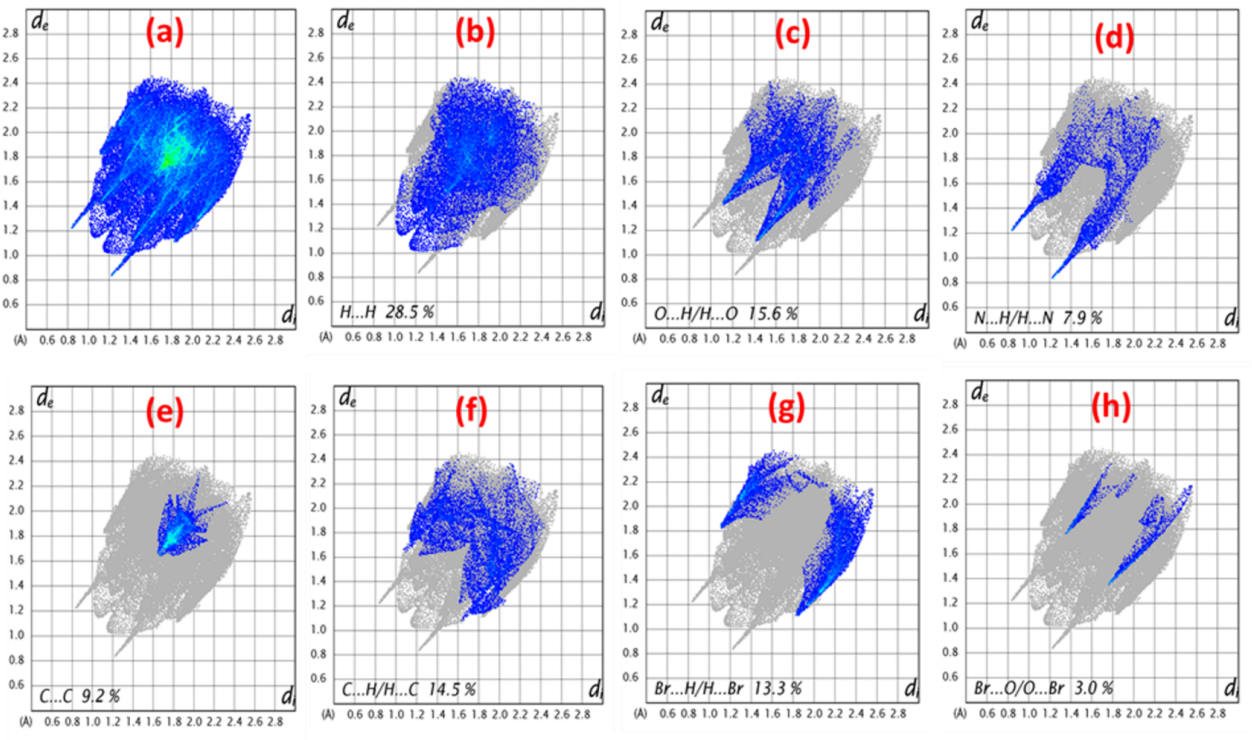

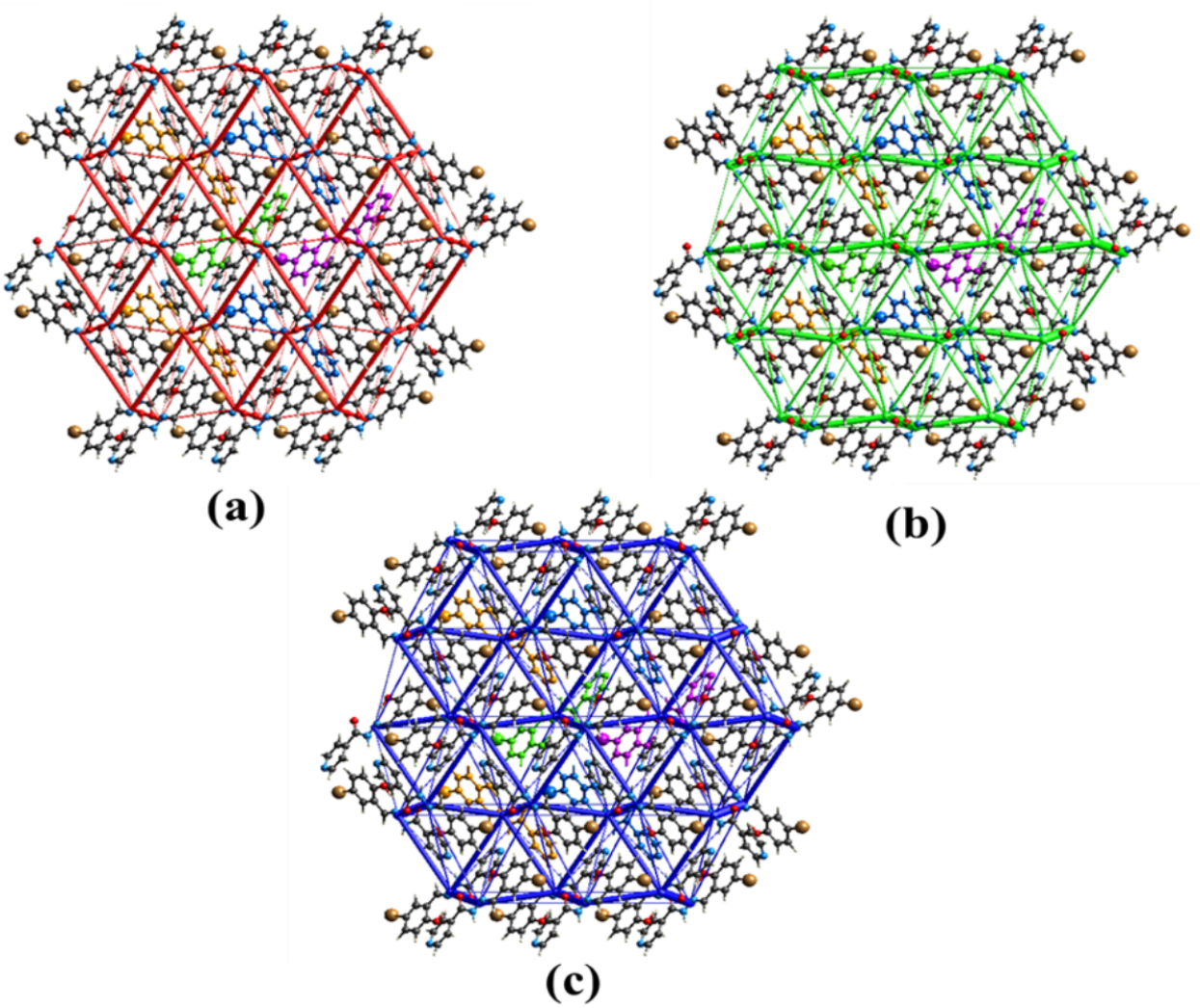
(a)
(b)
(c)

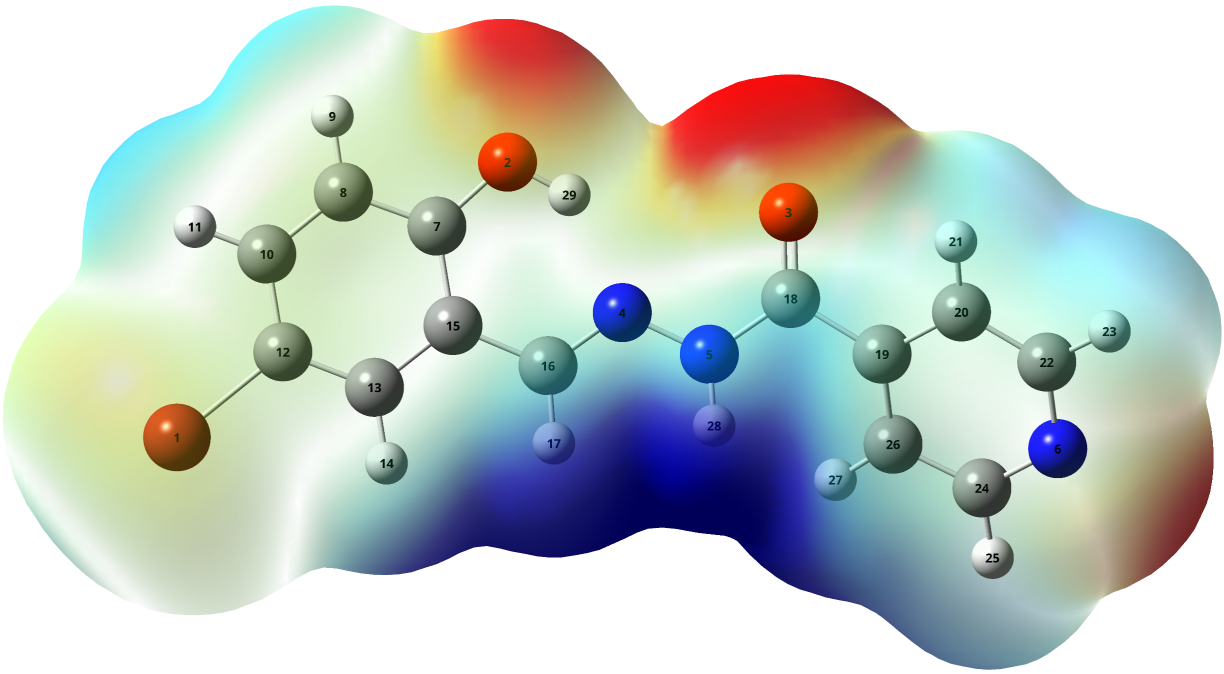

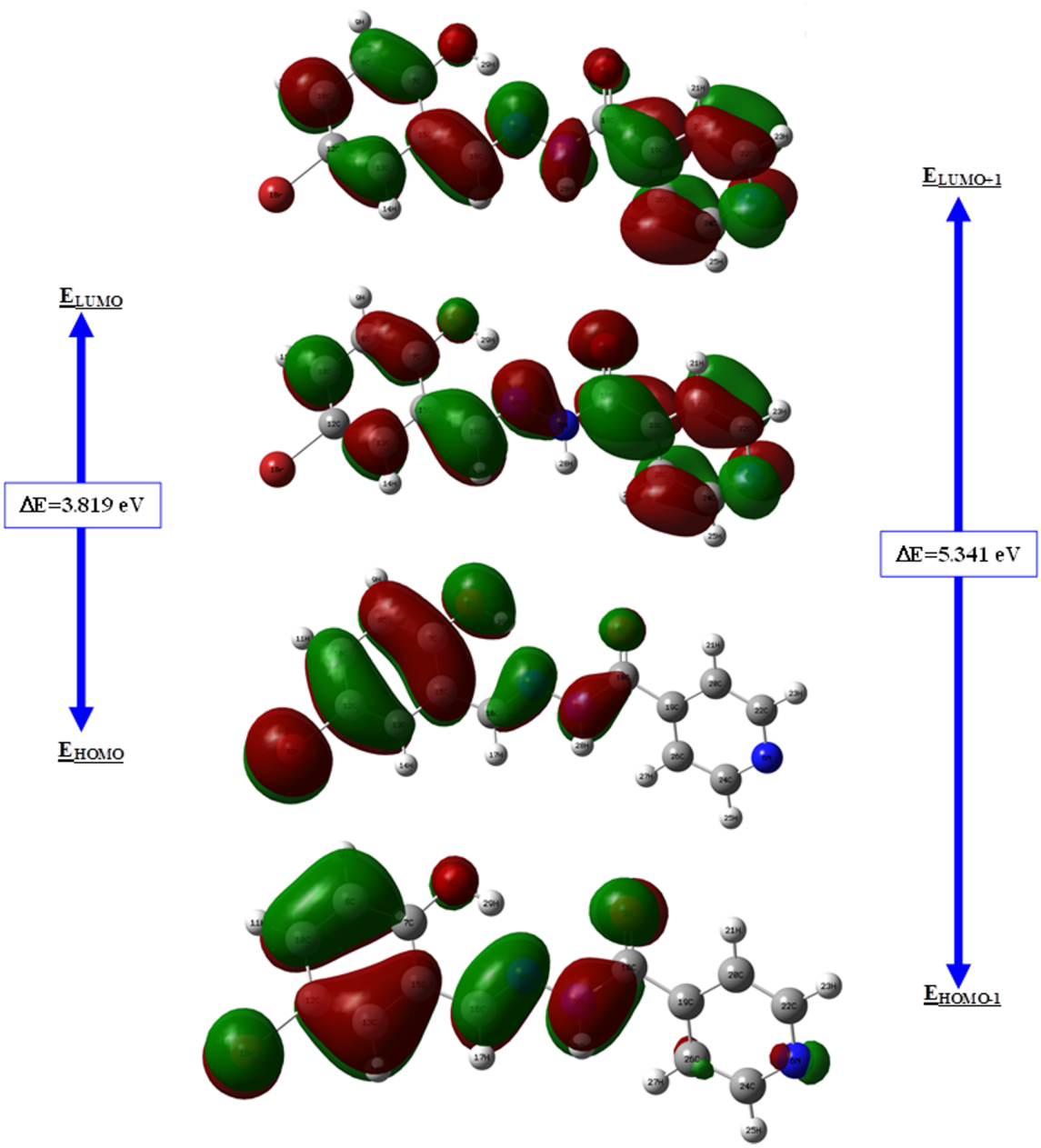
E_LUMO
ΔE=3.819 eV
E_HOMO
E_LUMO-1
ΔE=5.341 eV
E_HOMO-1

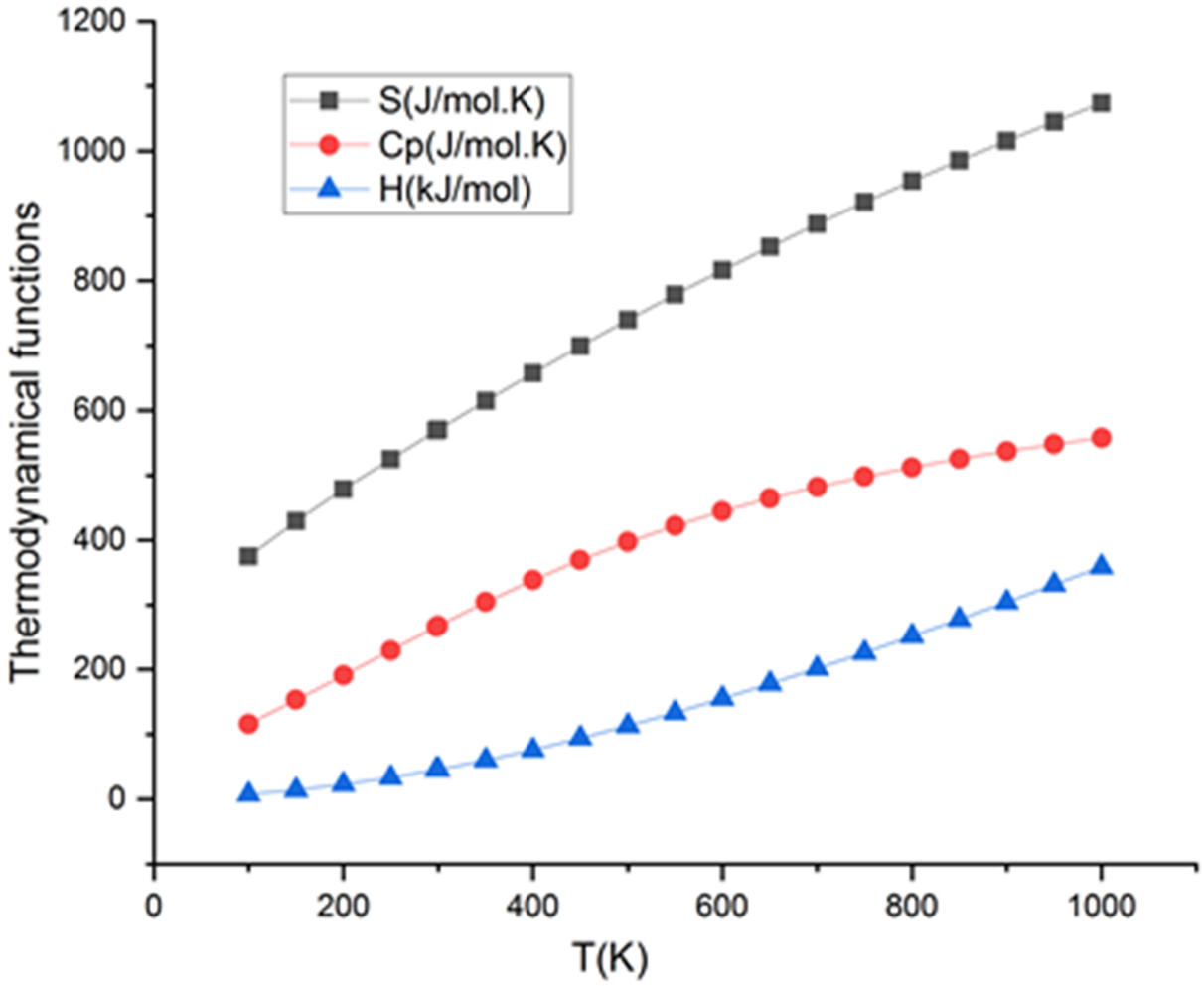
S(J/mol.K)
Cp(J/mol.K)
H(kJ/mol)
Thermodynamical functions
T(K)
0
200
400
600
800
1000
1200

**Highlights**

- A new isoniazid hydrazone was synthesized and characterized by spectroscopic methods.
- The molecular geometry, HOMO-LUMO energies and thermodynamic properties were explored using DFT/B3LYP method.
- Hirshfeld and MEP surfaces analyses were investigated.
- *In vitro* anti-diabetic activity against α-glucosidase and α-amylase enzymes were tested.
- Molecular docking studies confirmed the inhibitory activity of the title compound.

**Declaration of interests**

☒ The authors declare that they have no known competing financial interests or personal relationships that could have appeared to influence the work reported in this paper.

☐The authors declare the following financial interests/personal relationships which may be considered as potential competing interests: